One-Shot Polarization-Based Material Classification with Optimal Illumination

Miho Kurachi[1], Ryo Kawahara[2] [a] and Takahiro Okabe[3] [b]

[1]*Department of Artificial Intelligence, Kyushu Institute of Technology, Iizuka, Fukuoka 820-8502, Japan*
[2]*Graduate School of Informatics, Kyoto University, Sakyo-ku, Kyoto 606-8501, Japan*
[3]*Information Technology Track, Okayama University, Kita-ku, Okayama 700-8530, Japan*

Keywords: Material Classification, Polarization, Illumination, Margin Maximization.

Abstract: Image-based classification of surface materials is important for machine vision applications such as visual inspection. In this paper, we propose a novel method for one-shot per-pixel classification of raw materials on the basis of polarimetric feature such as the degree of linear polarization (DoLP) and the angle of linear polarization (AoLP). It is known that the polarimetric feature depends not only on the intrinsic properties of surface materials but also on the directions and wavelengths of light sources. Accordingly, our proposed method jointly optimizes the non-negative light source intensities for feature extraction and the discriminant hyperplane in the feature space via margin maximization so that the appearances of different materials are discriminative. We conducted a number of experiments using real images captured by using a light stage, and show that our method using a single input image works better than/comparably to the existing methods using a single/multiple input images.

1 INTRODUCTION

Classifying material categories such as metals and plastics, materials themselves such as iron and aluminum, and their surface states such as rust, cracks, and scratches are important for computer vision applications such as visual inspection of metallic surfaces (Zheng et al., 2002; Pernkopf and O'Leary, 2003) and printed circuit boards (Tominaga and Okamoto, 2003; Ibrahim et al., 2010). In this study, we focus on planar and unpainted raw materials, and achieve appearance-based *per-pixel* material classification that works in a *non-contact* and *non-destructive* manner.

The polarimetric properties of reflected light such as the degree of linear polarization (DoLP) and the angle of linear polarization (AoLP) play important roles for material classification (Wolff, 1990; Chen and Wolff, 1998). It is known that the DoLP of the reflected light depends on the refractive index of a surface material and differently behaves for specular and diffuse materials, and the AoLPs of specular and diffuse materials are different by $\pi/2$ (Shurcliff,

1962). The latter is because specular reflectance (reflectivity)/diffuse reflectance (transmissivity) is maximal when the polarization direction is perpendicular/parallel to the outgoing plane according to the Fresnel equations.

In general, the reflected light observed on an object surface consists of a diffuse reflection component and a specular reflection component, and the mixture ratio of those components depends also on the illumination condition. Specifically, the mixture ratio depends on both the direction and wavelength of a light source through the roughness and spectral reflectance of the surface. Therefore, the apparent DoLP and AoLP depends not only on the *intrinsic* properties, *i.e.* the refractive index, roughness, and spectral reflectance of the object surface but also on the directions and wavelengths of light sources (Kondo et al., 2020; Ichikawa et al., 2023).

Accordingly, we propose a novel method for polarization-based per-pixel material classification with the optimal illumination. We consider the 7D polarimetric feature space on the basis of the polarimetric image captured by using a polarization camera with a four linear polarization filter. We show the relationship between the illumination condition, *i.e.* the intensities of multi-spectral and multi-directional

[a] https://orcid.org/0000-0002-9819-3634
[b] https://orcid.org/0000-0002-2183-7112

light sources and the polarimetric feature, and *jointly* optimize both the illumination condition for *feature extraction* and the *discriminant hyperplane* in the feature space via margin maximization. Moreover, we impose the non-negativity constraints on the light source intensities, and achieve one-shot material classification that is applicable to dynamic objects as well.

The existing techniques for polarization-based material classification (Chen et al., 2009; Liang et al., 2022) often assume passive illumination, and then do not optimize the illumination condition under which input images are taken. In the context of material classification based on grayscale/color images (Gu and Liu, 2012; Liu and Gu, 2014; Wang and Okabe, 2017), the illumination condition is optimized so that the appearances of different materials are discriminative, but they do not utilize polarimetric clues. In contrast to those existing methods, our proposed method takes both the polarimetric clues and the illumination condition into consideration.

To confirm the effectiveness of our proposed method, we conducted a number of experiments using the images captured by using a polarization camera and an LED-based light stage, *i.e.* multi-spectral and multi-directional light sources. We show that the performance of our method using a single input image is better than/comparable to those of the existing methods using a single/multiple input images.

The main contributions of this study are twofold. First, we propose a novel method for one-shot per-pixel material classification based on the polarimetric clues under the optimal illumination. Specifically, we show the relationship between the intensities of multi-spectral and multi-directional light sources and the polarimetric feature, and jointly optimize both the non-negative illumination condition for feature extraction and the discriminant hyperplane in the feature space via margin maximization. Second, we experimentally show that our method using a single input image works better than/comparably to the existing methods using a single/multiple input images.

2 RELATED WORK

2.1 Polarization-Based Classification

In general, the reflected light observed on an object surface consists of a diffuse reflection component and a specular reflection component. It is known that the DoLP of the reflected light depends on the refractive index of a surface material and differently behaves for specular and diffuse components, and the AoLPs of those components are different by $\pi/2$ (Shurcliff,

1962). The seminal works by Wolff (Wolff, 1990) and Chen and Wolff (Chen and Wolff, 1998) study those properties of specular and diffuse reflection components, and propose polarization-based methods for classifying metals and dielectrics. Unfortunately, however, their methods require a number of images taken under varying polarization states, and then have difficulties in classifying materials of objects in motion.

The polarimetric properties are often combined with the other modalities for material classification. Chen *et al.* (Chen et al., 2009) show the effectiveness of multi-spectral and polarimetric imaging for classifying material categories. Recently, Liang *et al.* (Liang et al., 2022) show the effectiveness of multi-spectral and polarimetric images for material segmentation. They assume passive illumination, and then do not optimize the illumination condition under which input images are taken. On the other hand, our proposed method optimizes active illumination so that the appearances of different materials are discriminative, since the polarimetric properties such as DoLP and AoLP depends not only on the intrinsic properties of the object surface but also on the directions and wavelengths of light sources.

2.2 Illumination Optimization

In general, the coded illumination using multiple light sources is efficient in terms of SNR (Signal-to-Noise Ratio) and the number of required images. It is shown that the coded illumination is effective for image acquisition (Schechner et al., 2003), BRDF (Bidirectional Reflectance Distribution Function) measurement (Ghosh et al., 2007), shape recovery (Ma et al., 2007), and spectral reflectance recovery (Park et al., 2007). Whereas those methods optimize the coded illumination for reconstructing signals with high SNRs, our proposed method optimizes the illumination condition in terms of discriminative ability.

The coded illumination is utilized also for material classification. Gu and Liu (Gu and Liu, 2012) and Liu and Gu (Liu and Gu, 2014) propose an approach to per-pixel classification of raw materials based on spectral BRDFs. Specifically, they optimize the intensities of multi-spectral and multi-directional light sources for two/multi-class classification via linear SVMs/Fisher LDA. Unfortunately, however, their methods require two/multiple images taken under actual light sources with non-negative intensities, since they allow the optimal intensities could be negative. Wang and Okabe (Wang and Okabe, 2017) achieve per-pixel material classification from a single color image by jointly optimizing the light source inten-

sities and the disctiminant hyperplane with the non-negative constraints on the light source intensities. In contrast to those methods, our method takes account of the polarimetric clues as well as the illumination condition into consideration.

3 PROPOSED METHOD

3.1 Setup

Similar to the existing techniques (Gu and Liu, 2012; Liu and Gu, 2014; Wang and Okabe, 2017), we assume that objects of interest are planar and unpainted raw materials. Our proposed method illuminates those objects by using a light stage with L light sources, and then capture the images of them by using a polarization camera with a four linear polarization filter. We denote the four pixel values observed at a certain surface point through the four linear polarization filter ($0°$, $45°$, $90°$, and $135°$) by i_1, i_2, i_3, and i_4[1]. Unless otherwise noted, we omit the pixel's index since we address per-pixel classification.

Our proposed method uses the L images, each of which is captured under each light source, for training. On the other hand, our method uses a single image, which is captured under the L light sources with the optimal intensities, for test.

3.2 Two-Class Classification

Feature Space and Discriminant Hyperplane:
We consider the 7D polarimetric feature on the basis of the polarimetric image as $(i_1, i_2, i_3, i_4, \rho, c, s)^\top$. Here, ρ is the DoLP, $c = \cos(2\phi)$, and $s = \sin(2\phi)$ respectively, where ϕ ($-\pi/2 \leq \phi \leq \pi/2$) is the AoLP. Note that c and s are continuous at $\phi = \pm\pi/2$.

Our proposed method finds the linear discriminant hyperplane defined by

$$\sum_{d=1}^{4} w'_d i_d + ||\boldsymbol{w}||_2 (w'_5 \rho + w'_6 c + w'_7 s) + b = 0 \quad (1)$$

in the 7D feature space. Here, we call the set of light source intensities $\boldsymbol{w} = (w_1, w_2, w_3, ..., w_L)^\top$ the light source vector and the set of the weights of the polarimetric features $\boldsymbol{w}' = (w'_1, w'_2, w'_3, ..., w'_7)^\top$ the polarimetric vector, and b is the bias. We explain the reason why the 2-norm of the light source vector $||\boldsymbol{w}||_2$ is required later.

Polarimetric Feature and Illumination:
We denote the four set of pixel values observed under each of the L light sources with unit intensity as $\boldsymbol{x}_d = (x_{d1}, x_{d2}, x_{d3}, ..., x_{dL})^\top$ ($d = 1, 2, 3, 4$). According to the superposition principle of illumination, the pixel value i_d captured under the L light sources is represented as

$$i_d = \boldsymbol{w}^\top \boldsymbol{x}_d \quad (2)$$

by using the light source vector $\boldsymbol{w}$. Note that eq.(2) is the projection from $4L$-dimensional space to 4D space, and it acts as the feature extraction.

Substituting eq.(2) into eq.(1), we can rewrite the linear discriminant hyperplane as

$$\sum_{d=1}^{4} w'_d \boldsymbol{w}^\top \boldsymbol{x}_d + ||\boldsymbol{w}||_2 \times$$
$$(w'_5 \rho(\boldsymbol{w}) + w'_6 c(\boldsymbol{w}) + w'_7 s(\boldsymbol{w})) + b = 0. \quad (3)$$

Here, $\rho(\boldsymbol{w})$, $c(\boldsymbol{w})$, and $s(\boldsymbol{w})$ explicitly describe that those features depend on the light source vector $\boldsymbol{w}$, but we omit ($\boldsymbol{w}$) unless otherwise noted to make the notation simpler.

Joint Optimization:
Our proposed method jointly optimizes both the illumination condition, *i.e.* the light source vector $\boldsymbol{w}$ and the discriminant hyperplane, *i.e.* the pair of the polarimetric vector $\boldsymbol{w}'$ and the bias b via margin maximization. In the 7D feature space, the distance between a point $(i_1, i_2, i_3, i_4, \rho, c, s)^\top$ and the discriminant hyperplane in eq.(3) is given by

$$\frac{|\sum_{d=1}^{4} w'_d \boldsymbol{w}^\top \boldsymbol{x}_d + ||\boldsymbol{w}||_2 (w'_5 \rho + w'_6 c + w'_7 s) + b|}{||\boldsymbol{w}||_2^2 ||\boldsymbol{w}'||_2^2}.$$
$$(4)$$

Note that we can set the numerator to 1 for the set of points nearest to the discriminant hyperplane, *i.e.* support vectors without loss of generality in the same manner as the formulation of SVMs (Vapnik, 1998). This is because both the first and second terms of the numerator are proportional to the overall scales of $\boldsymbol{w}$ and $\boldsymbol{w}'$.

Hence, the optimization results in

$$\min_{\boldsymbol{w}, \boldsymbol{w}', b, \{\xi_n\}} \frac{1}{2} ||\boldsymbol{w}||_2^2 ||\boldsymbol{w}'||_2^2 + \frac{\alpha}{N} \sum_{n=1}^{N} \xi_n \quad (5)$$

subject to

$$y_n \left[\sum_{d=1}^{4} w'_d \boldsymbol{w}^\top \boldsymbol{x}_{nd} + ||\boldsymbol{w}||_2 \times \right.$$
$$\left. (w'_5 \rho_n + w'_6 c_n + w'_7 s_n) + b \right] \geq 1 - \xi_n$$

$$(n = 1, 2, 3, ..., N), \quad (6)$$
$$\xi_n \geq 0 \quad (n = 1, 2, 3, ..., N), \quad (7)$$
$$w_l \geq 0 \quad (l = 1, 2, 3, ..., L). \quad (8)$$

Here, y_n and ξ_n are the label (+1 or -1) and the slack variable of the n-th sample. We denote the number of training samples and the weight of the penalty term by N and α/N respectively. In order to achieve one-shot classification, we impose the non-negativity constraints on the light source intensities in eq.(8).

We use an alternative optimization technique for solving the above optimization, because when one of the light source vector $\boldsymbol{w}$ and the pair of the polarimetric vector and the bias $\{\boldsymbol{w}', b\}$ is fixed, it approximately results in the quadratic programming with respect to the other. Specifically, we iteratively update one of them; we fix $\boldsymbol{w}$ and update $\{\boldsymbol{w}', b\}$ via quadratic programming, and then we fix $\{\boldsymbol{w}', b\}$ and $\{\rho(\boldsymbol{w}), c(\boldsymbol{w}), s(\boldsymbol{w})\}$ by using $\boldsymbol{w}$ computed at the previous iteration and update $\boldsymbol{w}$ via quadratic programming. In our current implementation, we set the initial condition of the light source vector $\boldsymbol{w}$ to $(1, 1, 1, ..., 1)^{\top}$.

3.3 Multi-Class Classification

Combination of Two-Class Classification:
We combine the two-class classifiers for multi-class classification on the basis of binary tree. Let us consider 4-class classification for example. First, we find the two-class classifier that discriminates the four classes (A, B, C, and D) into $\{A, B\}$ and $\{C, D\}$. Second, we find the two-class classifier that discriminates A and B, and the two-class classifier that discriminates C and D. In general, we require $M = (K - 1)$ two-class classifiers for K-class classification.

Discriminant Hyperplanes:
In a similar manner to the two-class classifier formulated by eq.(3), we represent the m-th ($m = 1, 2, 3, ..., M$) linear discriminant hyperplane as

$$\sum_{d=1}^{4} w'_{md} \boldsymbol{w}^{\top} \boldsymbol{x}_d + ||\boldsymbol{w}||_2 \times$$
$$(w'_{m5}\rho(\boldsymbol{w}) + w'_{m6}c(\boldsymbol{w}) + w'_{m7}s(\boldsymbol{w})) + b_m = 0. \quad (9)$$

Here, $\boldsymbol{w}'_m$ and b_m are the m-th polarimetric vector and bias. Note that we achieve one-shot multi-class classification by sharing a *single* light source vector $\boldsymbol{w}$ among M classifiers.

Joint Optimization:
We jointly optimize the light source vector $\boldsymbol{w}$ and the set of the polarimetric vector and bias $\{\boldsymbol{w}'_m, b_m\}$ ($m = 1, 2, 3, ..., M$) in a similar manner to the two-class classification. Specifically, the joint optimization is for-
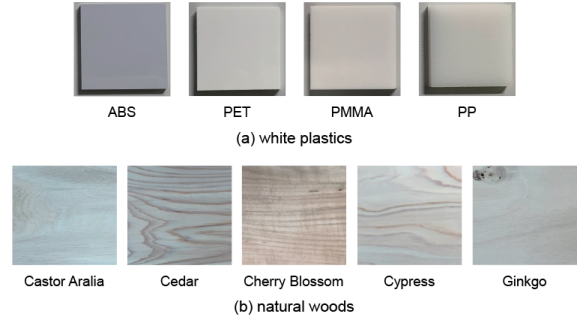

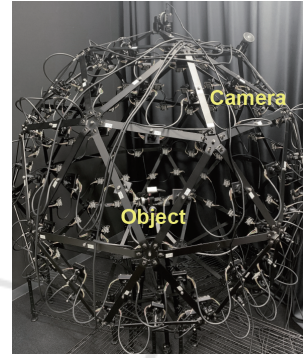Figure 1: Two sets of raw materials with similar appearances: (a) white plastics and (b) natural woods.

Figure 2: Our Kyutech-OU light stage II for illuminating an object of interest located at the center.

mulated as

$$\min_{\boldsymbol{w}, \boldsymbol{w}'_m, b, \{\xi_{mn}\}} \sum_{m=1}^{M} \left(\frac{1}{2} ||\boldsymbol{w}||_2^2 ||\boldsymbol{w}'_m||_2^2 + \frac{\alpha}{N} \sum_{n=1}^{N} \xi_{mn} \right) \quad (10)$$

subject to

$$y_{mn} \left[\sum_{d=1}^{4} w'_{md} \boldsymbol{w}^{\top} \boldsymbol{x}_{mnd} + ||\boldsymbol{w}||_2 \times \right.$$
$$\left. (w'_5\rho_{mn} + w'_6 c_{mn} + w'_7 s_{mn}) + b_m \right] \geq 1 - \xi_{mn}$$
$$(m = 1, 2, 3, ..., M) \ (n = 1, 2, 3, ..., N), \quad (11)$$
$$\xi_{mn} \geq 0$$
$$(m = 1, 2, 3, ..., M) \ (n = 1, 2, 3, ..., N), \quad (12)$$
$$w_l \geq 0 \ (l = 1, 2, 3, ..., L). \quad (13)$$

In a similar manner to the two-class classification, we solve the above optimization via an alternative optimization technique. Specifically, we set the initial condition of the light source vector $\boldsymbol{w}$ to $(1, 1, 1, ..., 1)^{\top}$, and then iteratively update the set of $\{\boldsymbol{w}'_m, b_m\}$ ($m = 1, 2, 3, ..., M$) by fixing $\boldsymbol{w}$ and vice versa.

Table 1: The classification accuracies (%) of the two-class classification for the white plastics: ours, ours with fixed w', ours with fixed w, Gu and Liu, SegFormer with s_0, and SegFormer with (s_0, s_1, s_2) from left to right.

	Ours	Ours with fixed w'	Ours with fixed w	Gu and Liu	SegFormer with s_0	SegFormer with (s_0, s_1, s_2)
Number of images	single	single	single	two	single	single
ABS vs. PET	**100.00**	**100.00**	**100.00**	**100.00**	87.99	99.94
ABS vs. PMMA	**100.00**	**100.00**	**100.00**	**100.00**	94.75	83.15
ABS vs. PP	99.94	**100.00**	99.88	**100.00**	99.61	90.38
PET vs. PMMA	**100.00**	99.94	86.22	96.27	53.28	50.67
PET vs. PP	**100.00**	**100.00**	**100.00**	**100.00**	99.87	83.96
PMMA vs. PP	**100.00**	**100.00**	**100.00**	**100.00**	99.66	99.98

Table 2: The classification accuracies (%) of the two-class classification for the natural woods: ours, ours with fixed w', ours with fixed w, Gu and Liu, SegFormer with s_0, and SegFormer with (s_0, s_1, s_2) from left to right.

	Ours	Ours with fixed w'	Ours with fixed w	Gu and Liu	SegFormer with s_0	SegFormer with (s_0, s_1, s_2)
Number of images	single	single	single	two	single	single
Castor Aralia vs. Ginkgo	**100.00**	99.96	98.36	99.60	99.28	99.97
Cedar vs. Cypress	**99.16**	99.10	75.36	98.90	51.45	53.65
Cedar vs. Cherry Blossom	**99.74**	99.44	98.00	99.26	97.52	93.76
Cypress vs. Ginkgo	**97.30**	94.12	80.74	92.82	91.18	83.04

4 EXPERIMENTS

In this Section, we explain our experimental setup, and then report our experimental results for two-class classification and multi-class classification. We show that the effectiveness of our proposed method is remarkable, especially for more challenging scenarios, *i.e.* one-shot multi-class classification.

4.1 Experimental Setup

We tested two sets of raw materials with similar appearances. One is the set of 4 white plastics: ABS, PET, PMMA, and PP in Figure 1 (a). The other is the set of 5 natural woods: Castor Aralia, Cedar, Cherry Blossom, Cypress, and Ginkgo in Figure 1 (b). We can see that the texture of Cedar, Cherry Blossom, and Cypress are more prominent than that of Castor Aralia and Ginkgo.

We captured the images of those objects by using a polarization camera of BFS-U3-51S5P-C from FLIR and our Kyutech-OU light stage II in Figure 2. Similar to the existing light stages (Gu and Liu, 2012; Liu and Gu, 2014; Wang and Okabe, 2017), the light stage consists of the LED clusters at different directions, and each cluster has narrow-band LEDs with different spectral intensities. In our experiments, we used the images taken under $92 \ (= L)$ light sources; 23 directions $\times$ 4 spectral intensities.

To confirm the effectiveness of our proposed method, we compared the performances of the following six methods:

- **Ours:** Our method jointly optimizes the light source vector w for feature extraction and the polarimetric vector w' (and the bias b) for the discriminant hyperplane in the feature space. Ours achieves one-shot classification by imposing the non-negative constraints on the light source intensities.

- **Ours with fixed w':** This method is used for the ablation study of the polarimetric feature. Specifically, we fix the polarimetric vector as $w' = (1/4, 1/4, 1/4, 1/4, 0, 0, 0)^\top$ in our method. In other words, it uses the s_0 component of the Stokes vector under the optimized illumination.

- **Ours with fixed w:** This method is used for the ablation study of the illumination optimization. Specifically, we fix the light source vector as $w = (1, 1, 1, ..., 1)^\top$ in our method. In other words, it uses the polarimetric feature under the unoptimized illumination.

- **Gu and Liu (Gu and Liu, 2012):** This method optimizes the light source intensities for material classification on the basis of SVMs. Because the non-negativity constraints are not imposed on the light source intensities, it requires two images for two-class classification, and $(K + 1)$ images for K-class classification when it combines two-class classification in a one-vs-the-rest manner. In other words, it require an additional image for compensating virtual light sources with negative intensities.

- **SegFormer (Xie et al., 2021) with s_0:** SegFormer

Table 3: The classification accuracies (%) of the four-class classification for (a) the white plastics and (b) the natural woods: ours, ours with fixed w', ours with fixed w, Gu and Liu, SegFormer with s_0, and SegFormer with (s_0, s_1, s_2) from left to right.

	Ours	Ours with fixed w'	Ours with fixed w	Gu and Liu	SegFormer with s_0	SegFormer with (s_0, s_1, s_2)
Number of images	single	single	single	five	single	single
(a) White plastics	**99.88**	91.13	94.41	90.72	71.93	68.24
(b) Natural woods	87.91	81.02	72.06	**96.49**	68.48	68.02

is one of the state-of-the-art methods based on transformer. To investigate the performance of the deep learning-based method with intensity images, the input to SegFormer is the s_0 component of the Stokes vector when $w = (1, 1, 1, ..., 1)^\top$.

- **SegFormer (Xie et al., 2021) with** (s_0, s_1, s_2)**:** To investigate the performance of the deep learning-based method with polarimetric images, the input to SegFormer is the s_1, s_2, and s_3 components of the Stokes vector when $w = (1, 1, 1, ..., 1)^\top$.

We used the MATLAB implementation (quadprog) of the inter-point-convex algorithm for the first iteration followed by the active-set algorithm (Gill et al., 1981) for the alternative optimization of eq.(5) and eq.(10). We empirically set the parameter α in those equations to 10^6 and 10^5 for the datasets of white plastics and natural woods respectively. For all of the above methods, we used 900/2,500 pixels per plastics/woods material in the test phase. In the training phase, we used the other 400 pixels per material for the above methods other than SegFormer.

We used 48 images with 900 pixels/88 images with 2,500 pixels per plastics/woods material for training SegFormer. We found that the performance of SegFormer tends to depend on the initial conditions to some extent. Then, we show the average of five trials for the results of SegFormer in Section 4.2 and Section 4.3.

4.2 Two-Class Classification

First, in Table 1, we summarize the accuracies of the two-class classification for the white plastics: ours, ours with fixed w', ours with fixed w, Gu and Liu (Gu and Liu, 2012), SegFormer (Xie et al., 2021) with s_0, and SegFormer with (s_0, s_1, s_2) from left to right. Note that Gu and Liu requires two input images taken under different illumination conditions but the other methods use only a single image per tow-class classifier in the test phase. We tested the six pairs of the four plastics: ABS vs. PET, ABS vs. PMMA, ABS vs. PP, PET vs. PMMA, PET vs. PP, and PMMA vs. PP from top to bottom.

Basically, we can see that the classification of the white plastics is relatively easy. Although the accuracies are often saturated, we can see that ours works
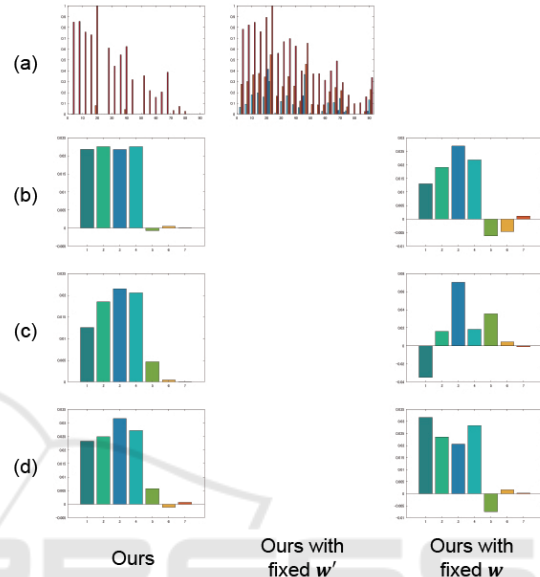

Figure 3: The optimized parameters for the four-class classification of the white plastics: Ours, Ours with fixed w', and Ours with fixed w from left to right, and (a) the light source vector w and the polarimetric vectors (b) w'_1, (c) w'_2, and (c) w'_3.

better than ours with fixed w and Gu and Liu with two input images. In addition, Table 1 also shows that ours outperforms SegFormer with s_0 and (s_0, s_1, s_2); it supports the effectiveness of the illumination optimization.

Second, we summarize the accuracies of the two-class classification for the natural woods in Table 2. We tested the four pairs of the five natural woods: Castor Aralia vs. Ginkgo, Cedar vs. Cypress, Cedar vs. Cherry Blossom, and Cypress vs. Ginkgo from top to bottom. We can see that our proposed method works better than the other methods. Since the classification of the natural woods is more difficult than the white plastics due to spatially-varying reflectance properties, the effectiveness of our method is more significant.

4.3 Multi-Class Classification

First, in Table 3 (a), we summarize the accuracies of the four-class classification for the white plastics:
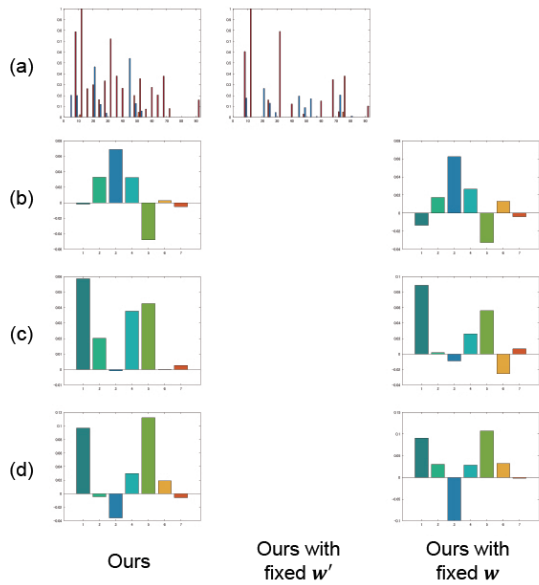
Figure 4: The optimized parameters for the four-class classification of the natural woods: Ours, Ours with fixed w', and Ours with fixed w from left to right, and (a) the light source vector w and the polarimetric vectors (b) w'_1, (c) w'_2, and (c) w'_3.
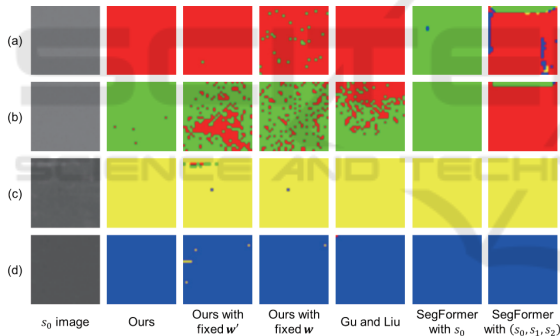

Figure 5: The s_0 image and the labels of the white plastics predicted by using the 6 methods: (a) PET, (b) PMMA, (c) PP, and (d) ABS. Red, green, yellow, and blue stand for PET, PMMA, PP, and ABS respectively.

ours, ours with fixed w', ours with fixed w, Gu and Liu (Gu and Liu, 2012), SegFormer (Xie et al., 2021) with s_0, and SegFormer with (s_0, s_1, s_2) from left to right. Note that Gu and Liu requires five input images taken under different illumination conditions but the other methods use only a single image in the test phase.

Comparing the performance of ours and those of ours with fixed w' and ours with fixed w, we can see the effectiveness of the joint optimization of the light source vector w for feature extraction and the polatimetric vector w' (and the bias b) for the discriminant hyperplane in the feature space. In addition, we can
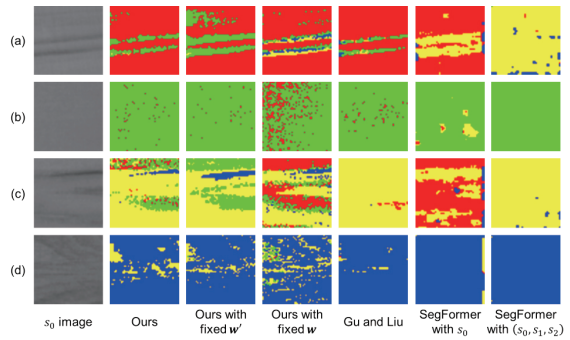

Figure 6: The s_0 image and the labels of the natural woods predicted by using the 6 methods: (a) Cypress, (b) Ginkgo, (c) Cedar, and (d) Castor Aralia. Red, green, yellow, and blue stand for Cypress, Ginkgo, Cedar, and Castor Aralia respectively.

see that ours with a single input image works better than Gu and Liu with five input images. Table 3 (a) also shows that ours outperforms SegFormer with s_0 and (s_0, s_1, s_2).

Figure 3 shows the light source vectors and the polarimetric vectors of ours, ours with fixed w', and ours with fixed w from left to right. We can see that our light source vector is significantly different from $(1, 1, 1, ..., 1)^\top$, but our polarimetric vector is not so different from $(1/4, 1/4, 1/4, 1/4, 0, 0, 0)^\top$. Therefore, for the white plastics, we can see that the optimization of illumination condition is more important than the use of the polarimetric feature.

Second, we summarize the accuracies of the four-class classification for the natural woods in Table 3 (b). The four materials are Castor Aralia, Cedar, Cypress, and Ginkgo. Similar to the case of the white plastics, we can see the effectiveness of the joint optimization of the light source vector w and the polatimetric vector w' (and the bias b), because ours works better than ours with fixed w', and ours with fixed w. We can also see that ours outperforms SegFormer with s_0 and (s_0, s_1, s_2). Since the classification of the natural woods is more difficult than the white plastics due to spatially-varying reflectance properties as shown in Figure 5 and Figure 6, the effectiveness of our method is more significant. Note that Gu and Liu performs best but requires five input images.

Figure 4 shows the light source vectors and the polarimetric vectors of ours, ours with fixed w', and ours with fixed w from left to right. We can see that our light source vector and polarimetric vector are significantly different from $(1, 1, 1, ..., 1)^\top$ and $(1/4, 1/4, 1/4, 1/4, 0, 0, 0)^\top$. Therefore, we can see that both the illumination optimization and the polarimetric feature are important for classifying the natural woods.

5 CONCLUSION

In this paper, we proposed a novel method for one-shot per-pixel material classification based on the polarimetric clues under the optimal illumination. Specifically, we show the relationship between the intensities of multi-spectral and multi-directional light sources and the polarimetric feature, and jointly optimize both the non-negative illumination condition for feature extraction and the discriminant hyperplane in the feature space via margin maximization. Then, we experimentally showed that our method using a single input image works better than/comparably to the existing methods using a single/multiple input images.

The future work of this study includes the extension to complex objects such as non-planar surfaces and translucent materials with significant subsurface scattering. The use of the other modalities such as polarimetric light sources is another direction of our future work.

ACKNOWLEDGEMENTS

REFERENCES

Chen, C., Zhao, Y., Luo, L., Liu, D., and Pan, Q. (2009). Robust materials classification based on multispectral polarimetric brdf imagery. In *SPIE Proceedings*, volume 7384, pages 220–227.

Chen, H. and Wolff, L. (1998). Polarization phase-based method for material classification in computer vision. *IJCV*, 28(1):73–83.

Ghosh, A., Achutha, S., Heidrich, W., and O'Toole, M. (2007). BRDF acquisition with basis illumination. In *Proc. IEEE ICCV2007*, pages 1–8.

Gill, P., Murray, W., and Wright, M. (1981). *Practical Optimization*. Academic Press.

Gu, J. and Liu, C. (2012). Discriminative illumination: per-pixel classification of raw materials based on optimal projections of spectral BRDF. In *Proc. IEEE CVPR2012*, pages 797–804.

Ibrahim, A., Tominaga, S., and Horiuchi, T. (2010). Spectral imaging method for material classification and inspection of printed circuit boards. *Optical Engineering*, 49(5):057201.

Ichikawa, T., Fukao, Y., Nobuhara, S., and Nishino, K. (2023). Fresnel microfacet BRDF: Unification of polari-radiometric surface-body reflection. In *Proc. IEEE/CVF CVPR2023*, pages 16489–16497.

Kondo, Y., Ono, T., Sun, L., Hirasawa, Y., and Murayama, J. (2020). Accurate polarimetric BRDF for real polarization scene rendering. In *Proc. ECCV2020*, pages 220–236.

Liang, Y., Wakaki, R., Nobuhara, S., and Nishino, K. (2022). Multimodal material segmentation. In *Proc. IEEE/CVF CVPR2022*, pages 19800–19808.

Liu, C. and Gu, J. (2014). Discriminative illumination: per-pixel classification of raw materials based on optimal projections of spectral BRDF. *IEEE Trans. PAMI*, 36(1):86–98.

Ma, W.-C., Hawkins, T., Peers, P., Chabert, C.-F., Weiss, M., and Debevec, P. (2007). Rapid acquisition of specular and diffuse normal maps from polarized spherical gradient illumination. In *Proc. EGSR2007*, pages 183–194.

Park, J.-I., Lee, M.-H., Grossberg, M., and Nayar, S. (2007). Multispectral imaging using multiplexed illumination. In *Proc. IEEE ICCV2007*, pages 1–8.

Pernkopf, F. and O'Leary, P. (2003). Image acquisition techniques for automatic visual inspection of metallic surfaces. *NDT&E International*, 36:609–617.

Schechner, Y., Nayar, S., and Belhumeur, P. (2003). A theory of multiplexed illumination. In *Proc. IEEE ICCV2003*, pages 808–815.

Shurcliff, W. (1962). *Polarized Light: Production and Use*. Harvard University Press.

Tominaga, S. and Okamoto, S. (2003). Reflectance-based material classification for printed circuit boards. In *Proc. IEEE ICIAP2003*, pages 238–244.

Vapnik, V. (1998). *Statistical Learning Theory*. Wiley-Interscience.

Wang, C. and Okabe, T. (2017). Joint optimization of coded illumination and grayscale conversion for one-shot raw material classification. In *Proc. BMVC2017*.

Wolff, L. (1990). Polarization-based material classification from specular reflection. *IEEE Trans. PAMI*, 12(11):1059–1071.

Xie, E., Wang, W., Yu, Z., Anandkumar, A., Alvarez, J., and Luo, P. (2021). SegFormer: Simple and efficient design for semantic segmentation with transformers. In *Proc. NeurIPS2021*, pages 12077–12090.

Zheng, H., Kong, L., and Nahavandi, S. (2002). Automatic inspection of metallic surface defects using genetic algorithms. *Journal of Materials Processing Technology*, 125–126:427–433.